International Journal of Advanced Interdisciplinary Sciences

Vol.1, Issue.1, August 2021,72-92

Molecularly imprinted graphene oxide/gold nanoparticle-based polymer for the adsorption and photocatalytic degradation of 2,4-Dichlorophenoxyacetic acid

Deepa J. R.[a*], Amritha Ghosh. S[a], Sree Remya T. S.[a], Jeneena K.B.[a]

a. Department of Chemistry, Sree Narayana College, Kollam, India

*Corresponding author: deepanguram2008@gmail.com

Abstract

Water contamination via. the indiscriminate usage of pesticide in agricultural field is a major health issue faced by the modern society. 2,4-Dichlorophenoxyacetic acid (2, 4-D) is a widely used pesticide and herbicide which kills pests, weeds, insects etc. It is highly toxic to human and also cause irritation to eye and skin. The toxicity of these pesticides is gradually polluting our water resources. Hence, the removal of pesticide from various water resources is very important. Currently, many methods are available for the purification of water such as adsorption, ultrafiltration, osmosis etc. Among them, adsorption followed by Advanced Oxidation Process (AOP) is considered to be more effective for the removal of organic impurity, their degradation with high efficiency and lower energy consumption for the disposal of adsorbed materials. In the present work, molecularly imprinted graphene oxide/gold nanoparticle grafted vinyl trimethoxy silane copolymerised with itaconic acid/ 2-hydroxyethyl methacrylate (GO/AuNP-g-VTMS-Co-IA/HEMA) polymer was synthesized for effective adsorption and photodegradation of 2,4-D. It was characterised using Fourier Transform Infrared Spectroscopy (FTIR) X-ray diffraction analysis (XRD), scanning electron microscope (SEM), (DRS), Energy-dispersive X-ray spectroscopy (EDS). Adsorption and degradation studies were conducted to substantiate efficacy and effectiveness of pesticide removal.

Keywords: Adsorption; Advanced Oxidation Process, Molecular imprinted polymers; Photodegradation

Article History: Received 19 June 2021; Revised 20 August 2021; Accepted 25 August 2021; Published 31 August 2021.

1. Introduction

The excess use of pesticides agriculture to kill different types of pests heavily contaminates our water resources. 2, 4-dichlorophenoxyacetic acid (2, 4 -D) is the oldest and most widely available herbicide [1] found to be capable of selectively killing weeds. It is also used in laboratories for plant research as a supplement in plant cell cultural media. The toxicity of these pesticides gradually polluted water resources, creates toxicological and health issues [2]. As per World Health Organisation (WHO), the maximum permissible contaminant level of the pesticide is 20 μg/l in drinking water [3,4]. Commonly used method for the detection of 2, 4-D in drinking water is HPLC (High Performance Liquid Chromatography) coupled with an UV (Ultraviolet) detector [5]. using methods like filtration, coagulation, flocculation, sedimentation, distillation, electrochemical treatment and ion exchange [6-7]. Among the methods used to remove pesticides from water, adsorption is the widely accepted technique due to low-cost, reproducibility, availability and easy to handle [8]. After the removal of organic pollutants from the water removal of the same from the adsorbent is possible by advanced oxidation process (AOP),which have advantages like higher efficiency and lower energy consumption for the disposal of adsorbed materials [9]. AOP involves photocatalytic degradation through the production of reactive species (hydroxyl radicals [OH]) can oxidize organic pollutants [10]. Graphene based materials are excellent adsorbent materials which are used for the removal of pharmaceutical drugs, dyes, solvent rather than toxic chemicals and pesticides. Graphene oxide(GO) consists of many oxygen function groups mainly epoxy, hydroxyl and CO. GO is hydrophilic in nature and its surface contains large number of negative charges [11-14]. Graphene composites have light absorbing properties as a result of photo excitation. The excited electrons are moved from valence band to the conduction band. Graphene is a potential electron acceptor having 2-dimensional p-conjugation structures [15]. Graphene oxide based advanced polymers can have increased adsorption capacity and enable photo degradation in visible light through band gap of GO, nearly equal to 1.79 eV, that acted as p-type semiconductor photo catalyst [16]. In graphene oxide/gold nanoparticle composite (GO/AuNP composite), AuNP in combination with GO enhance the photocatalytic activity of GO. On doping GO with AuNP, band gap will be tuned around 2.1-2.9 eV range. Molecularly imprinted polymer (MIP) technique is used to create template shaped cavities in polymer matrices. Graphene Oxide is used for the preparation of conducting MIP. Gold nanoparticles (AuNP) are intercalated with GO in order to enhance the conductivity of GO. GO/AuNP can be silylated with allyl trimethyl silane (ATMS) resulting in a conducting polymer.

In the present work, itaconic acid and 2-hydroxy ethyl methacrylate have been used as monomers. Polymer synthesis involves graft copolymerisation of GO/AuNP with itaconic acid followed by radical polymerization of 2-hydroxy ethyl methacrylate and crosslinking with ethylene glycol dimethacrylate (EGDMA) resulting the composite GO/AuNP-g-VTMS-Co-IA/HEMA (Vinyl trimethoxy silane copolymerised with-itaconic acid/2-hydroxy ethyl methacrylate grafted graphene oxide/gold nano particle).

2. Materials and methods

2.1. Materials

Chloroauric acid $H[AuCl_4]$, sodium citrate, graphite powder, sulphuric acid (H_2SO_4), potassium permanganate ($KMnO_4$), methanol, hydrogen peroxide (H_2O_2), N, N-dimethyl formamide (DMF), potassium peroxo disulfate($K_2S_2O_8$) were purchased from E-Merck, India Ltd. 2,4-Dichlorophenoxyacetic acid was purchased from Alfa Aeser (England). Sodium hydroxide (NaOH), Itaconic acid, 2-Acrylamido-2-methyl propane sulfonic acid was purchased from Sigma Aldrich. Vinyl trimethoxy silane (VTMS), Ethylene glycoldimethacrylic acid (EGDMA) was purchased from Tokyo chemical industry co. Ltd. All aqueous solutions were prepared in double distilled water.

2.2 Preparation of adsorbent

Preparation of adsorbent GO/AuNP-g-VTMS-Co-IA/HEMA involve the steps described in the following paragraphs.

2.2.1. Preparation of graphene oxide

The graphite powder was grinded for 1.5 h using a motor and pestle. The graphite powder was mixed with conc. H_2SO_4 and $NaNO_3$ and stirred for 2.5 h in an ice water bath. Then, $KMnO_4$ was added to the above mixture and stirring continued for another 2.5 h till a gradual change in colour to mud dish brown was observed. The mixture was allowed to attain room temperature. Around 75 ml of distilled water was added into it and stirring was continued for another 30 minutes. H_2O_2 was added into the solution and stirred for 15 minutes. Then, the mixture was washed continuously using distilled water to bring the mixture to neutral level pH.

2.2.2. Preparation of gold nanoparticles (Au NP) & GO/AuNP composite

Gold nanoparticles were synthesised through Turkevich method [17]. 2 ml of 0.1M chloroauric acid $H[AuCl_4]$ was stirred for 15 min at 80 ℃ in 100 ml double distilled water. 10 mol of 0.01 M aqueous sodium citrate was added and stirred for 30 min at 80 ℃. A clear solution turned to vine red indicated the formation of gold nano sol (AuNP). GO was synthesised by modified

Hummer's method [18]. The GO/AuNP composite was prepared by shaking 0.1 g each of GO and AuNP in a beaker containing 100 ml of deionized water for 12 h.

2.2.3 Preparation of silynated GO/AuNP

About 0.4051 g of previously intercalated GO/AuNP was mixed with 4 ml dimethyl formamide (DMF). The mixture was dispersed thoroughly using ultrasonicator for 1.5 h. To this mixture about 0.4288 g of vinyl trimethoxy silane (VTMS) in 40 ml DMF was added drop wise for 1 hr and stirred for 12 h at 65 ℃ to facilitate silynation. The excess of DMF in the mixture was then decanted, the residue was washed with methanol for 2-3 times and dried in the oven. The resulting mixture was then finely powdered and stored.

2.2.4. Preparation of molecularly imprinted polymer (MIP)

For the synthesis of MIP, a pre polymerized mixture was prepared by adding 25 ml of DMF to about 0.5 g of 2,4-dichlorophenoxyacetic acid and continuously stirred for 30 min, followed by the addition of 1 ml of 2-hydroxy ethyl methacrylate and 1g of itaconic acid. The mixture was continuously stirred for 1.5 h. 0.9241 g potassium persulfate (KPS) was added into this mixture and continuously stirred for about an hour at 75 ℃. The pre-polymerization was facilitated with continuous stirring and addition of 5 ml of ethylene glycol methacrylate (EGDMA). The resulting polymer was then washed for several times with distilled water to completely remove the excess DMSO and KPS. The polymer was also washed with methanol to remove 2, 4-dichlorophenoxyacetic acid and washed thoroughly with distilled water in Soxhlet apparatus for 3 to 4 days and constantly checking the presence of 2, 4-D with the help of UV visible spectroscopy. The polymer was then dried, powdered, and stored.

The entire step involved in the preparation of MIP is given in **Scheme 1.**

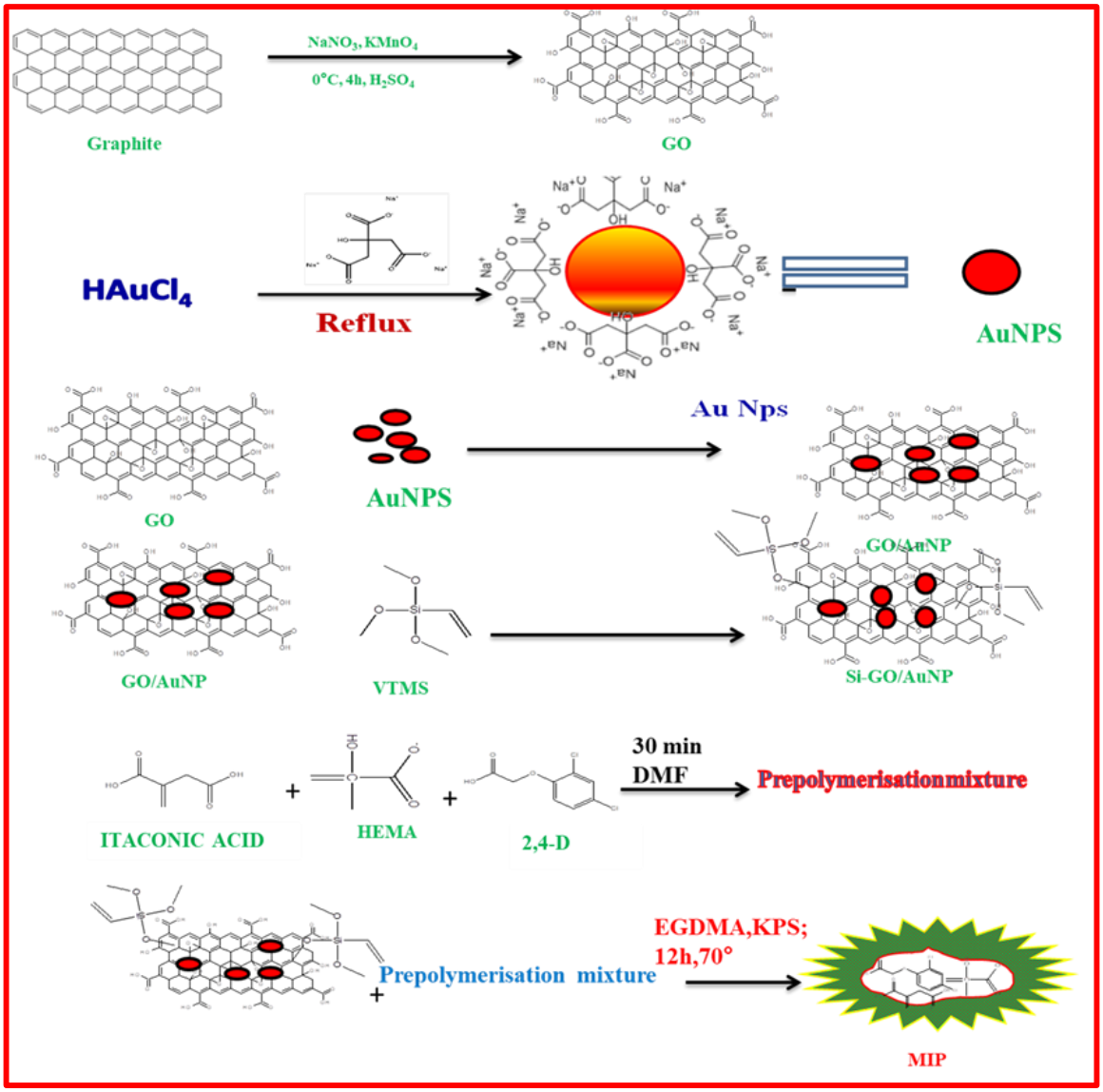

Scheme 1. Preparation of molecularly imprinted polymer

2.3 Instrumentation

All pH measurements were carried out using a systronic microprocessor pH metre (India, model-361). A temperature-controlled water bath shaker (Rotex, four techs shaking incubator) was used for equilibrium studies. The absorbance measurements were performed on a Perkin Elmer lambda 365 UV-Visible spectrometer. Infrared spectra were recorded on Agilent Technologies carry 630 FTIR spectrometer. X-ray powder diffraction patterns were recorded with D8 Advance Davinci X-ray Analyzer diffractometer. The surface morphology of adsorbent was studied using Zeiss EVO18 scanning electron microscope. EDX analysis was also performed on the same instrument. XPS spectra were taken using Thermo Scientific Esca lab XI+XPS system. DRS analysis were performed on Perkin Elmer/Visible NIR spectrometer lambda 950. Photocatalytic experiments were conducted using a solar simulator (AAA Solar light line A1, Science Tech. Pt. Ltd.)

2.4. Adsorption experiments

Batch experiments were performed by equilibrating 0.05 g of adsorbent with 25 ml 2,4-D solutions of predetermined initial concentrations. By adding NaOH and HCl of different concentrations, initial pH of the solutions was maintained at the required pH value. The suspensions were shaken for 3 h. The solid and liquid phases were separated by centrifugation at 6000 rpm for 15 min. The 2, 4-D concentrations in liquid phase were determined by UV/Visible Spectrophotometer at 266 nm. The amount of 2, 4-D adsorbed in (mg/g) at equilibrium (q_e) was calculated using mass balance equation as given below.

$$q_e = \frac{(C_0 - C_e)V}{W} \quad (1)$$

$$\text{Adsorption } \% = \frac{C_0 - Ce}{C_0} \times 100 \quad (2)$$

Where C_0 and C_e are the initial and final concentration of 2, 4-D in the solutions in (mg/L), V is the volume of the aqueous solution (mL) and W is the weight of GO/AuNP-g-VTMS-Co-IA/HEMA (g). All the adsorption experiments were done in triplicates and mean cumulative values were represented. The difference in results for triplicate measurements was less than 3.0%

2.5. Photo catalytic degradation of 2, 4-D

The photo catalytic degradation of 2, 4-D was done using Solar Simulator, A_1Solar light line having the intensity of 100 Mw/ cm^2. Two different concentrations of 2, 4-D (2.0, 4.0 mg/L) solution were taken in Erlenmeyer flasks (250 mL capacity), containing added 2 g/L of the adsorbent and the initial pH of the solution was adjusted. Then adsorption experiments were done in dark for 90 min to obtain equilibrium adsorption of 2, 4-D onto the photo catalyst. After this, the concentration of 2, 4-D was measured using UV-visible spectrophotometer at 266 nm, which is considered as C_0 (mg/L) at t = 0 for photo catalytic degradation experiment. The solution with the adsorbent was placed in the solar simulator in a wide vessel having specific surface area. The solutions were withdrawn at definite time intervals to determine the concentration of 2,4-D. The percentage removal of 2,4-D from the solution at different time intervals due to photo degradation was calculated using the equation:

$$Degraded\ 2{,}4-D(\%) = 100 - [\frac{c_0 - c}{c_0}]\ x100 \quad (3)$$

The effect of solution pH and presence of inorganic ions on the photo degradation efficiency of the photo catalyst was tested. All adsorption experiments were carried out in triplicate with standard deviation less than 2.0 %. The experimental data should be selected within the range of standard deviation of 2.0 %. The kinetic and isotherm parameters were obtained by a linear regression analysis using Origin pro 8.0 software.

3. Results and Discussion

3.2. Characterization of the adsorbent

3.2.1. FTIR Analysis

The FTIR spectra of GO, $AuCl_4$, AuNP, GO/AuNP, silynated GO/AuNP, MIP, MIP with 2,4-D, MIP without 2,4-D, NIP (Non-Imprinted Polymer) is given in **Figure 1**. The spectrum of GO shows characteristic peaks at 1470 cm^{-1} and 1500 cm^{-1}, that correspond to C-C stretching vibration of GO (presence of aromatic ring). A peak at 1720 cm^{-1} corresponds to stretching vibration of C=O. The graphite has characteristic peaks at 1300 cm^{-1} and 1507 cm^{-1}, that corresponds to C=C stretching vibration [17]. The IR spectrum of $AuCl_4$ shows a peak at 3270 cm^{-1} related to stretching vibration of C-H bonds. IR spectrum of AuNP shows a broad spectrum. A peak at 1249 cm^{-1} corresponds to CO stretching. A peak at 3270 cm^{-1} corresponds to OH stretching. In the IR spectrum of GO/AuNP, a peak at 1730 cm^{-1} corresponds to C=O stretching, while a peak at 3640 cm^{-1} corresponds to O-H stretching. The peak at 3640 cm^{-1} corresponds to O-H stretching, the decrease in the peak of silylated GO/AuNP indicates that silylation happened through OH functionality. Characteristic peaks of C=C, C-C aromatic stretching were observed at 1640 cm^{-1},1480 cm^{-1} in the MIP along with the peak at 1740cm^{-1} indicating the formation of Carboxyl group on polymer surface. These modifications in the IR spectrum of MIP compared to GO/ AuNP confirms the modifications happened via polymerisation on to the surface of GO/AuNP. In the FTIR spectrum of NIP, peak at 1145 cm^{-1} was due to the presence of Si-O-C bond, peaks at 1647 and 1723 cm^{-1} were due to the C=O stretching vibrations in IA. A band at 3410 cm^{-1} was due to the –OH stretching vibrations of carboxylic group. In the NIP spectrum, characteristic peaks of MIP were absent which demonstrated successful structural modification done on MIP. The absence of template selective binding cavities in NIP confirmed the proposed selectivity of the synthesized MIP.

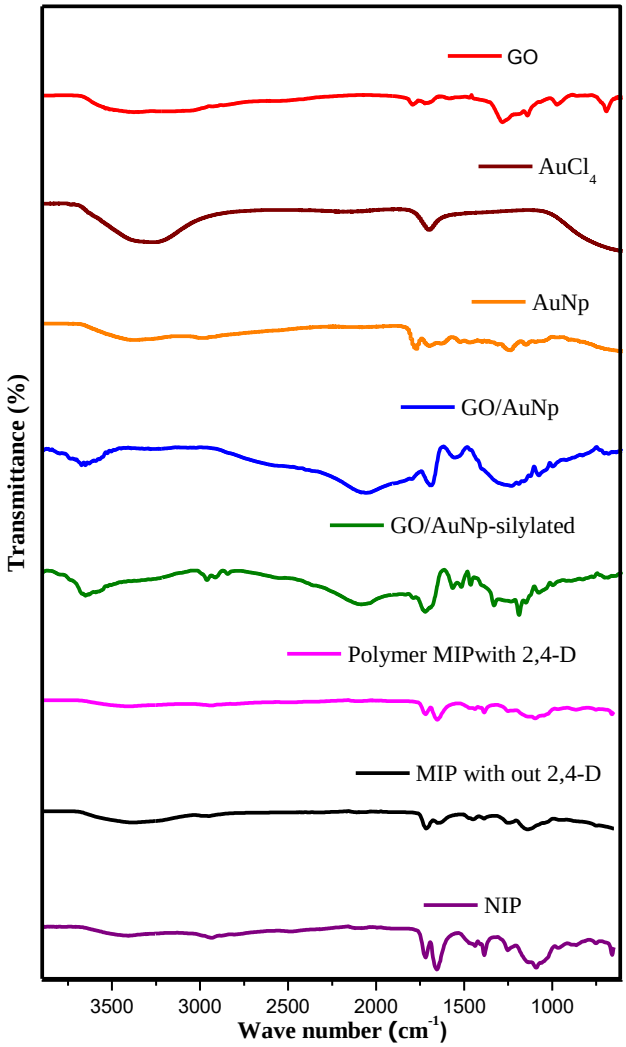

Figure 1. FTIR spectra of GO, $AuCl_4$, AuNP, GO/AuNP, silynated GO/AuNP, MIP with 2,4-D, MIP without 2,4-D and NIP

3.1.2 XRD Analysis

The XRD pattern of GO, GO/AuNP, MIP, MIP+2,4-D, and NIP are shown in **Figure 2.** GO shows sharp peak at 2θ value of 11.28^0 [18]. 2θ peak at 38.07^0, 26.20^0, 38.07^0, 29.8^0, 29.85^0 were observed for graphite, In GO/AuNP characteristic peak of GO at 11.28^0 disappeared and shows a specific peak at 38.07^0 indicates the composite formation of GO with AuNP. The X-ray diffraction pattern of MIP having more crystalline nature as compared to MIP with 2,4-D, as the peaks are more prominent as compared to MIP with2.4-D. due to crystalline nature of MIP, the more crystalline nature can attribute to the fact that specific recognition site is present on the polymeric surface. In the case of NIP no characteristic peaks are observed as the amorphous nature of NIP, may be due to the absence of specific recognition site.

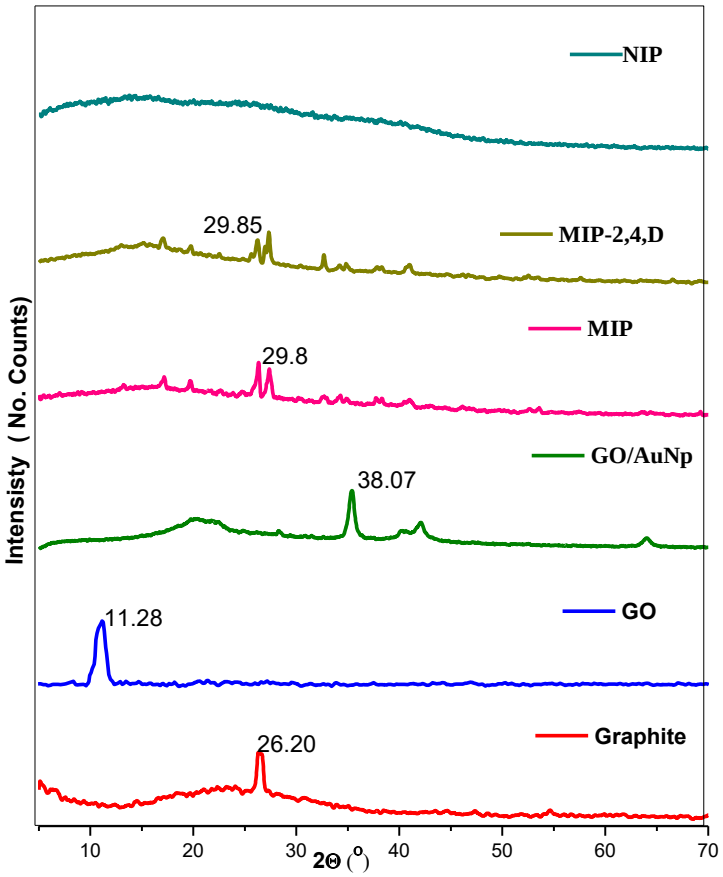

Figure 2. XRD patterns of Graphite, GO, GO/AuNP, MIP, MIP-2,4-D, NIP

3.1.3 SEM Analysis

Figure 3 shows the results of SEM analysis of GO, 2,4-D loaded MIP, MIP and NIP. The SEM images show different morphologies in each stage of synthesis. The morphological difference between MIP, 2,4-D loaded MIP and NIP can be clearly identified from the SEM images obtained. The image of GO having large surface area shows a sheet like morphology and agglomeration. Diameter of GO is 200 µm which indicates appreciably higher surface area of GO. Surface morphology of MIP is extremely different from that of GO. The presence of cavities indicates the presence of more porous surface due to the specific recognition site and the 2,4-D loaded MIP surface appear to be smoother because of the incorporation of template on to the specific site of MIP [3]. The attachment of template molecule changed the morphology as amorphous appearance compared to MIP. NIP possess entirely different morphology as that of MIP, due to absence of non-specific recognition site.

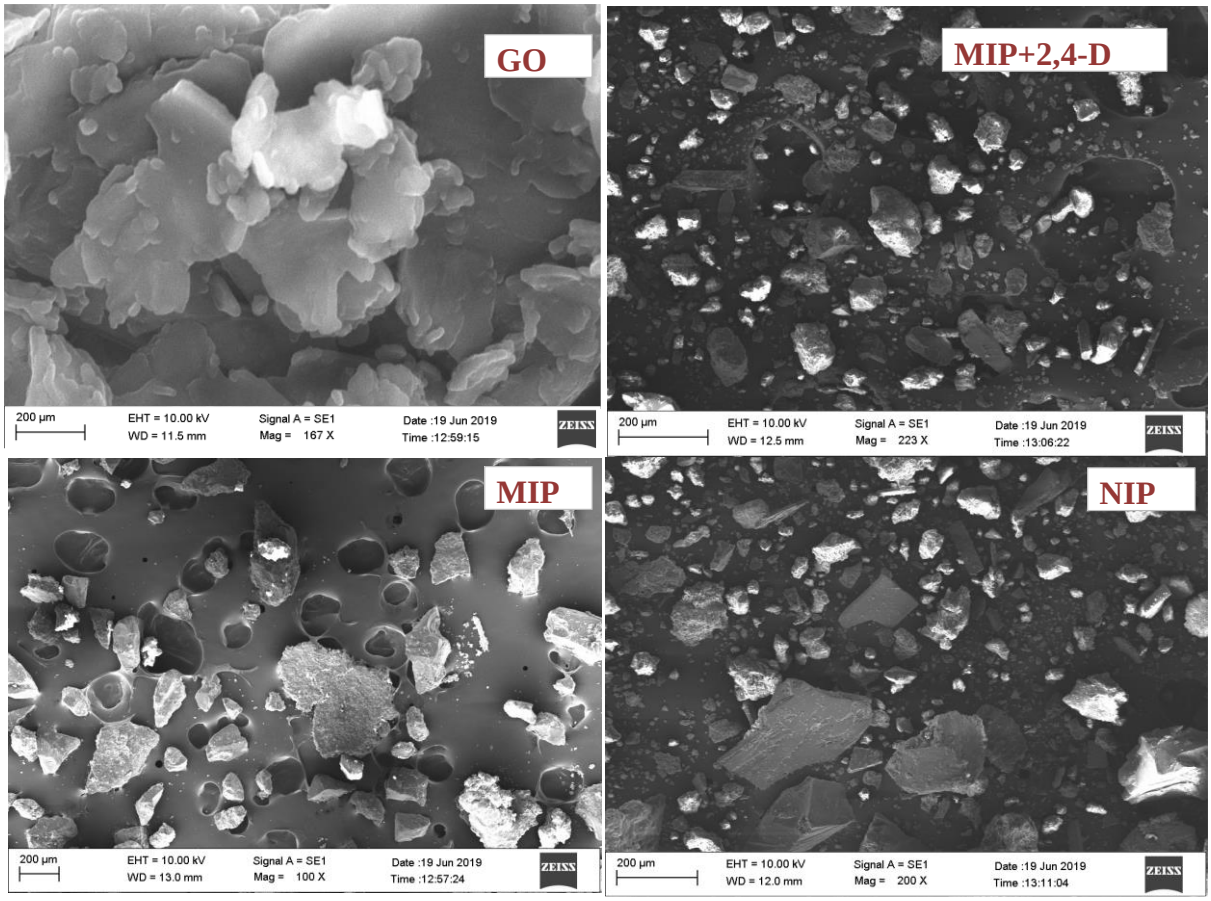

Figure 3. SEM images of GO, MIP+2,4-D, MIP, NIP

3.1.4 EDX Analysis

The EDS spectra of MIP and 2,4-D loaded MIP are given in **Figure 4.** In the spectra of MIP, the intensities of C and O are given and their percentage composition is given as 59.74 % and 30.72 % respectively. The presence of trace amount of sulphur, gold, nitrogen give the idea of successful modification of GO to the polymer. Besides C, H and O present in GO, MIP with 2,4-D has a higher percentage composition of carbon and oxygen. MIP without 2,4-D has lower percentage composition compared to the previous result. Trace amount of chlorine is also present (0.78 %). The EDS spectra provide clear idea about the incorporation of 2, 4-D in MIP, which could raise the composition percentage.

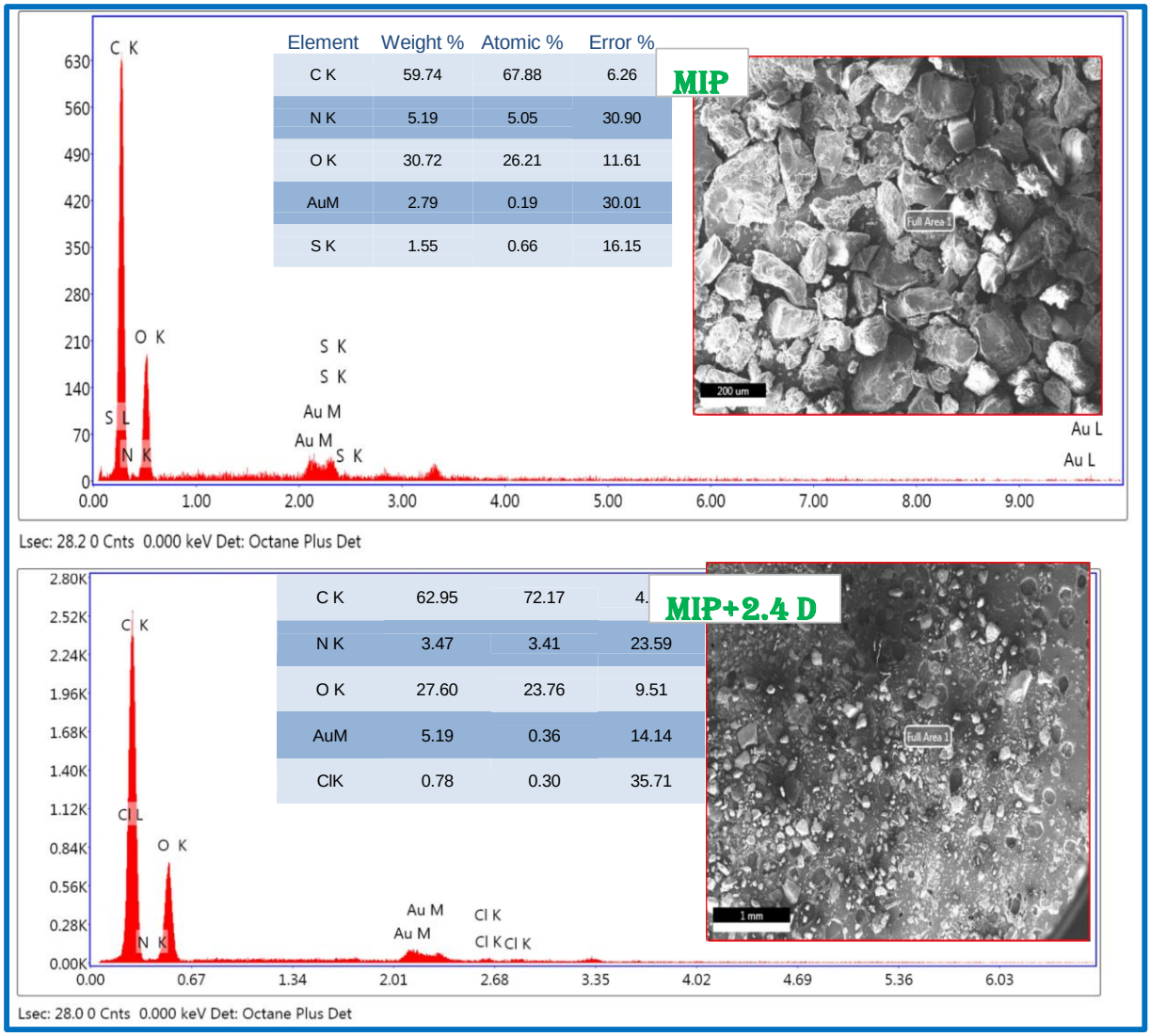

Figure 4. EDX patterns of MIP and MIP+2,4-D

3.1.5 DRS Analysis

The band gap energies of GO, GO/AuNP and MIP were obtained from Kubelka-Munk plots and were found to be 1.81, 2.43, 2.81 respectively **Figure 5**. The band gap of GO is 1.812 eV, and this band gap won't allow photocatalytic degradation in visible region. Hence on doping with AuNP, the band gap increased, and the value obtained was 2.43 eV. On converting GO to GO/AuNP, the band gap increasing to 2.43 eV and further converting GO/AuNP to MIP, the band gap lies below 3 eV and the value obtained was 2.81 eV. The perfect doping of GO/AuNP on MIP enhances the photocatalytic activity under visible light, due to electron transfer process.

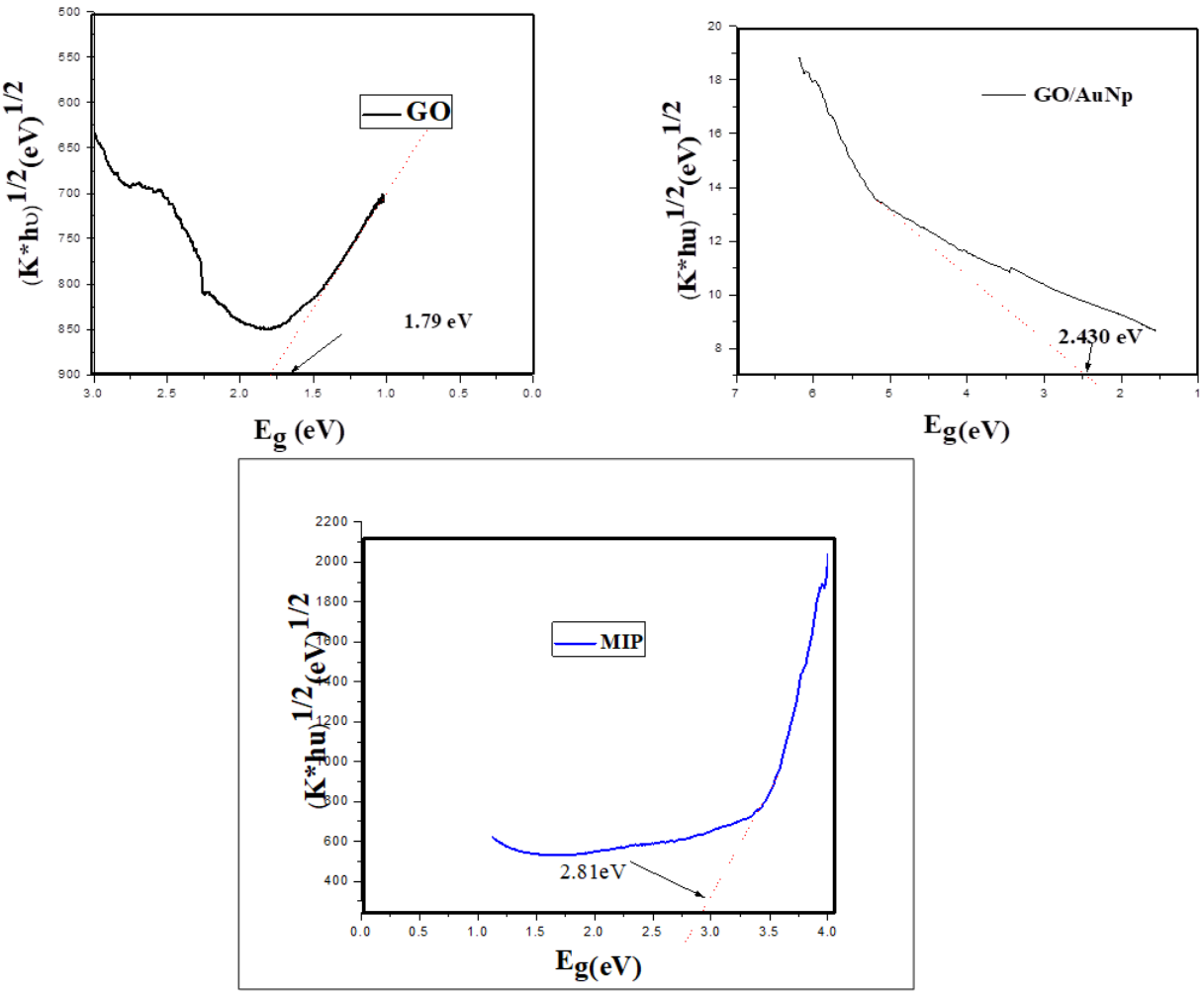

Figure 5. DRS patterns of GO, GO/AuNP and MIP

3.2 Adsorption Experiment

3.2.1 Optimization of pH

Adsorption efficiency of 2, 4-D on MIP is dependent on pH of the test solution. Aqueous solutions of 2, 4-D with pH ranging from 2 to 8 were prepared with two different initial concentration of 2 ppm and 4 ppm. The pH of the test solution was adjusted using 0.1 M HCl and 0.1M NaOH solutions. The response behaviour over the entire concentration range of 2, 4-D (2.0-11) was carried out. At pH 5.0, a maximum response was obtained. A graph was plotted with adsorption percentage of 2, 4-D against pH of the solution **Figure 6.** At very low pH values, the adsorption capacity was found to be low and between 35 % and 45 %. This is due to the weak interaction between 2, 4-D ions and H^+ ions. A gradual increase in adsorption capacity was observed with increasing pH value. The maximum adsorption of 2,4-D on MIP occurred at pH 5. The pka value of 2, 4-D is 2.6-3.3 [19] and at this pH range the functionality present on the surface of the material (COOH) exist as natural, above that limit it exists as

COO^-. Hydrogen bonding takes place between COOH group of the MIP and COOH group of the 2, 4-D, that will help the binding of 2, 4-D [3, 20]. Above the pH value of 5, the adsorption capacity of 2, 4-D decreases.

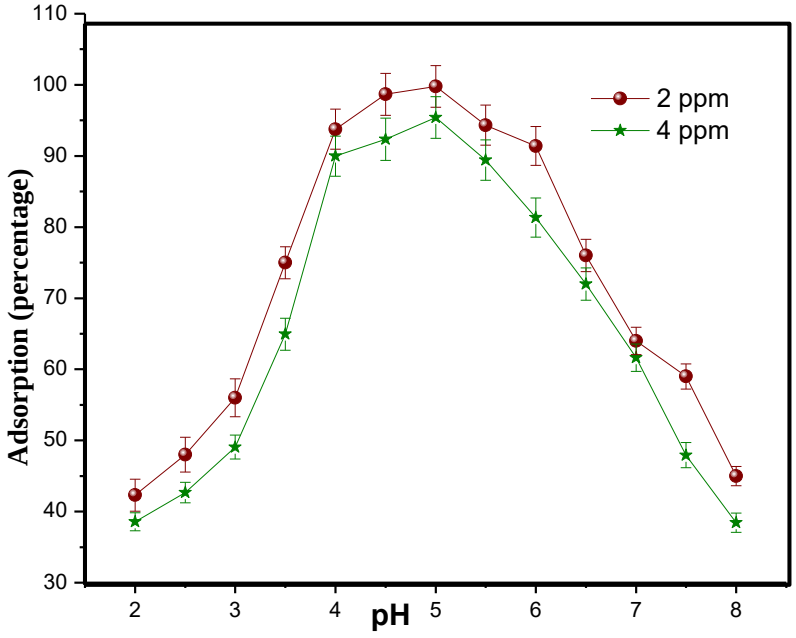

Figure 6. Optimization study of pH for the adsorption of 2,4-D on MIP

3.2.2 Adsorption kinetics

The effect of contact time on the adsorption of 2, 4-D on the GO/AuNP-g-VTMS-Co-IA/HEMA composite was studied in the concentrations of 2 and 8 mg/L. A graph is plotted with q_e against time [19]. The equilibrium time was reached at 50 min **Figure 7**. The adsorption rate was higher at initial stage, due to the greater number of reaction sites for the adsorption of 2, 4-D and concentration gradient. The initial concentration has any significant effect to reach equilibrium. As the initial concentration increases from 2 to 8 mg/L, the adsorption capacity increases from 0.9248 to 3.533 mg/g.

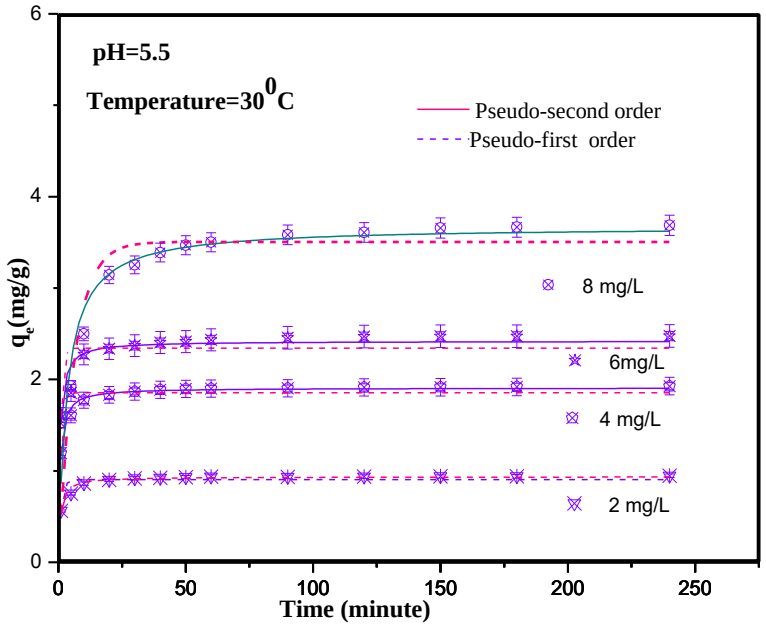

Figure 7. Adsorption kinetics

The experimental kinetics data can be interpreted using the non-linear kinetic equations given below:

$$q_t = q_e(1 - e^{-k_1 t}) \quad (4)$$

$$q_t = \frac{k_2 q_e^2 t}{1 + k_2 q_e t} \quad (5)$$

The results are shown in **Table 1**. The pseudo second order equation proved a good correlation with the experimental data. The values of R^2 and χ^2 reflect a better correlation for the pseudo second order model. The rate constant value k_2 decreases from 1.69 to 0.78 g/mg/min when the concentration increases from 2 to 8 mg/L. It is due to the absence of intermediate state formation during the adsorption process. The adsorption capacity agreed very well with both the experimental and the calculated values confirms physisorption like possible mechanism for the adsorption of 2, 4-D on the GO/AuNP-g-VTMS-Co-IA/HEMA composite.

Table 1. Kinetic parameters for the adsorption of 2, 4-D onto GO/AuNP-g-VTMS-Co-IA/HEMA

Concentration (mg/L)	q_e (mg/g) exp.	pseudo-first order				pseudo-second order			
		K_1 (min^{-1})	q_e (mg/g)	R^2	χ^2	k_2 (g/mg/min)	q_e (mg/g)	R^2	χ^2
2.0	0.981	0.96	0.9248±0.02	0.96	0.23	1.69	0.9855±0.02	0.99	0.69
4.0	1.965	1.54	1.855±0.03	0.94	3.14	0.98	1.917±0.03	0.99	0.98
6.0	2.589	1.87	2.369±0.02	0.93	4.15	0.86	2.569±0.02	0.99	0.68
8.0	3.988	1.85	3.533±0.03	0.91	5.47	0.78	3.914±0.03	0.99	0.56

3.3 Photocatalytic Degradation Experiment

3.3.1 Effect of pH on photodegradation

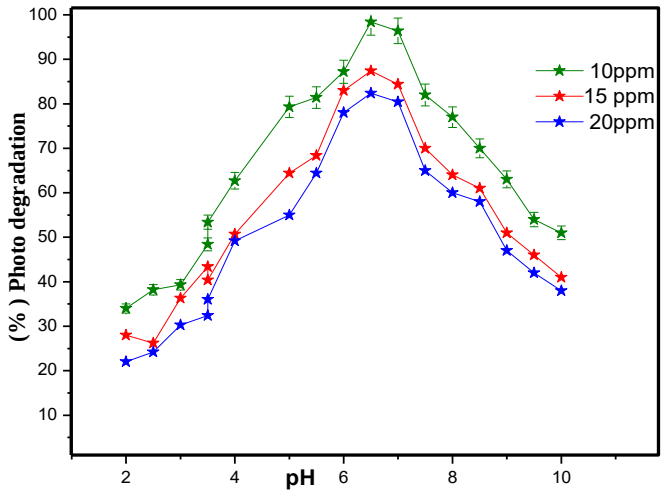

Figure 8. Effect of pH on photodegradation

Observing **Figure 8** it is clear that the photocatalytic degradation capacity depends on pH of the solution. The degradation of the pollutant was obtained at different pH values between the range 2-10. The experiment was conducted using 10 ppm, 15 ppm and 20 ppm of 2, 4-D solution The pH of the supernatant solution after adsorption was adjusted before photocatalytic degradation to know the effect of pH in the 2, 4-D degradation. At lower pH values, the degradation of 2, 4-D is not easier. But when the pH increased from 2 to 6.48, the photodegradation efficiency of the photocatalyst increases up to 90 %. Throughout this pH

range, there is an electrostatic interaction of 2, 4-D with the surface functional groups of photocatalyst. When the pH values range from 6.48 to 10, the degradation efficiency decreased from 90 to 30 %, due to the reduced interaction between the 2, 4-D molecule and the photocatalyst.

3.3.2 Photocatalytic Degradation Kinetics

For understanding enhanced photodegradation efficiency of the photocatalyst, photodegradation experiments were conducted with composite (GO), polymer (GO/AuNP-g-VTMS-Co-IA/HEMA) and without the catalyst (Blank) [21]. The experimental results are reported in **Figure 9**. From the figure, no photodegradation process was observed for blank. 2,4-D slightly degraded in presence of GO and could combine with 2,4-D in a lower rate, due to the recombination of electron-hole pairs. GO has large oxygen containing groups, due to its large surface area, AuNP-GO can enhance the degradation greater than GO and this may due to abundant oxygen functionalities. However, GO/AuNP-g-VTMS-Co-IA/HEMA enhance the degradation and almost completed it within 40 min.

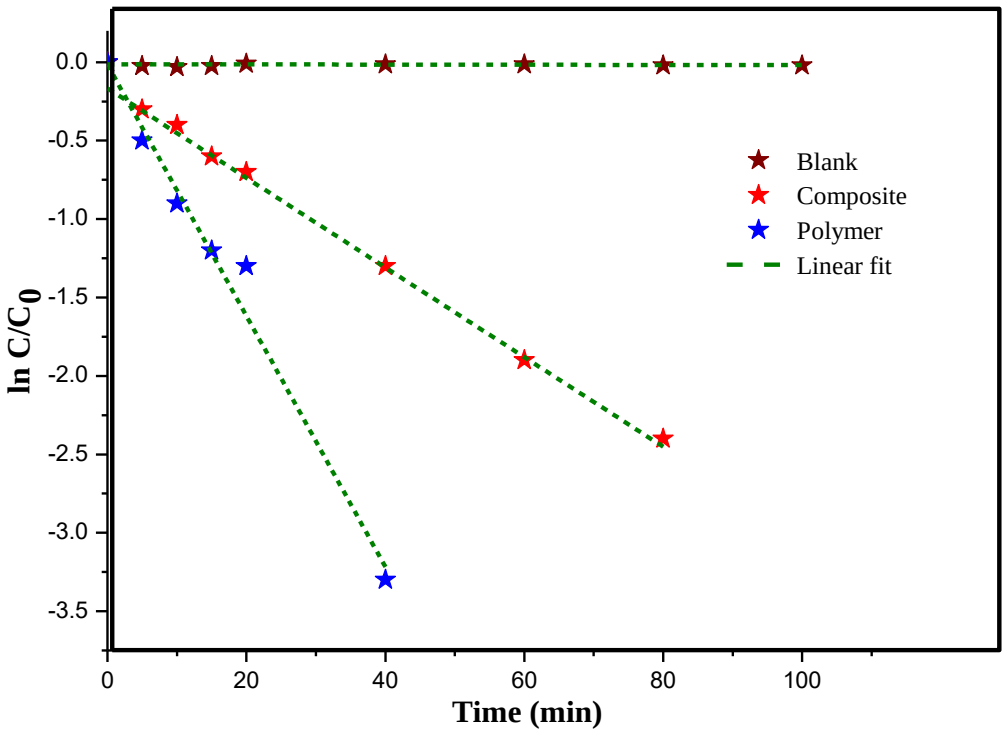

Figure 9. Photocatalytic Degradation Kinetics

3.3.3 Mechanism of Photodegradation

When GO/AuNP-g-VTMS-Co-IA/HEMA/2,4-D composite is irradiated by visible light with photon energy equal or higher than their band gaps, GO/AuNP-g-VTMS-Co-IA/HEMA /2,4-D composite is excited to generated electron-hole pairs. These changes move towards the surface during the degradation process. The 2,4-D adsorbed on the GO/AuNP-g-VTMS-Co-IA/HEMA surface is excited by visible light, and acts as photosensitizer, the molecule can eject electrons onto the conduction band of GO/AuNP-g-VTMS-Co-IA/HEMA/2,4-D system.

$$\text{GO/AuNP-g-VTMS-Co-IA/HEMA} + h\upsilon \longrightarrow \text{GO/ AuNP-g-VTMS-Co- IA/HEMA}(e_{CB}^- + h\upsilon_{CB}^+)$$

$$^1\text{2,4-D}^* \text{ or } ^3\text{2,4-D}^* + \text{GO/AuNP-g-VTMS-Co-IA/HEMA} \longrightarrow {}^1\text{2,4-D}^+ + \text{GO/AuNP-g-VTMS-Co-IA/HEMA}\ (e_{cb}^-) / {}^3\text{2,4-D}^+ + \text{GO/AuNP-g-VTMS-Co-IA/HEMA}\ (e_{cb}^-)$$

The photogenerated electrons are easily transferred from the valence band to the conduction band of GO/AuNP-g-VTMS-Co-IA/HEMA composite. The GO acts as electron sink and avoids the recombination of electron hole pairs and the holes can created readily on conduction band of GO/AuNP-g-VTMS-Co-IA/HEMA. During this photodegradation process, the electrons adsorbed O_2 and H_2O on the surface of GO/AuNP-g-VTMS-Co-IA/HEM A producing super oxide anion radical ($O_2^{\cdot -}$) [22]. Created holes expected to trap H_2O and adsorbed OH^- to produce $OH^{\cdot}$ species. These species are very strong oxidising and highly reactive agents, that can degrade Organic pollutant into harmless compounds (CO_2 and H_2O).

$$\text{GO/AuNP-g-VTMS-Co-IA/HEMA}\ (e_{CB}^-) + O_2 \longrightarrow O_2^{\cdot -} + \text{GO/AuNP-g-VTMS-Co-IA/HEMA}$$

$$\text{GO/AuNP-g-VTMS-Co-IA/HEMA}\ (h_{VB}^+) + H_2O \longrightarrow \text{GO/AuNP-g-VTMS-Co-IA/HEMA} + H^+ + OH^-$$

$$O_2^{\cdot -} + H^+ \longrightarrow HO_2^{\cdot +}$$

$$\text{GO/AuNP-g-VTMS-Co-IA/HEMA}\ (h_{VB}^+) + OH^- \longrightarrow \text{GO/AuNP-g-VTMS-Co-IA/HEMA} + OH^{\cdot}$$

$$OH^{\cdot} + \text{2,4-D} \longrightarrow \text{Degradation products}\ (H_2O + CO_2)$$

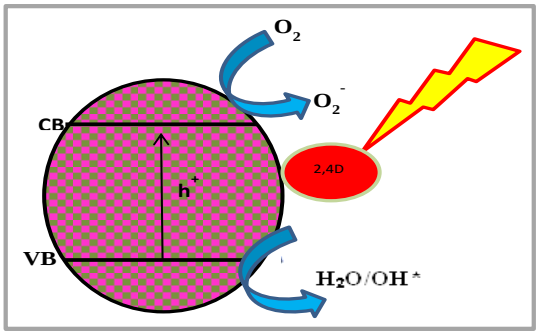

Figure 10. Mechanism of photodegradation of 2,4-D

3.4. Regeneration and reusability of photocatalyst

MIP was tested for its regeneration and recyclability. Five cycles of the photo catalytic experiment for photocatalyst were carried out with sunlight using 0.5 g of the adsorbent loaded with 2, 4-D from aqueous solution (0.4 g/L). The results are shown in **Figure 11** a reduction in the adsorption efficiency was experienced, since values of 97.6 % on first usage to 89.8 % after the fifth cycle of reuse were measured. The photocatalytic degradation capacity of the adsorbent was reduced from 93.09 % (first cycle) to 81.08 % (fifth cycle). 2, 4-D could be completely decomposed in each cycle and the photocatalyst did not exhibited any significant change in its photocatalytic activity during the repeated photo catalytic experiments [23]. It could conclude that the photocatalyst is suitable for reuse.

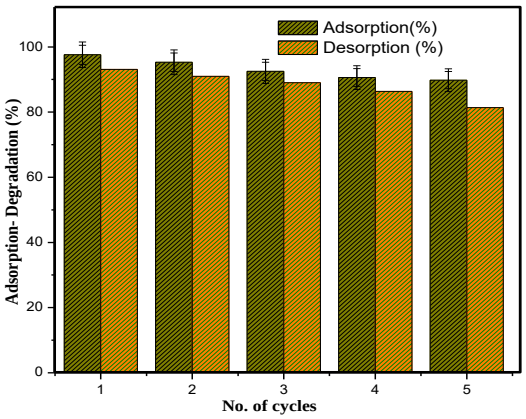

Figure 11. Adsorption–Degradation cycle of 2,4-D on to MIP

4. Summary and conclusions

For the adsorption and photo degradation of a pesticide (2, 4-D), a novel photo catalyst, GO/AuNP-g-VTMS-Co-IA/HEMA polymer was successfully synthesized and the photo degradation of 2, 4-D from water under visible light was investigated. The enhanced photo catalytic performance of GO/AuNP-g-VTMS-Co-IA/HEMA was related to the efficient photosensitized electron injection and repressed electron recombination in the GO/AuNP, due

to the electron-transfer process with GO as electron collector and transporter. These features make the GO/AuNP-g-VTMS-Co-IA/HEMA as a recommendable candidate for applications related to environmental aqueous pollution. Prepared photo catalyst was characterized by means of SEM, XRD, FTIR, DRS and EDS techniques. SEM images showing morphology of each stages up to the final composite gave the idea of successful modification through the polymerisation. EDX results showed the successful incorporation of 2, 4-D in MIP. DRS result also explains the successful modification and the stability of composite by measuring the different band gaps of GO, GO/AuNP, MIP. On doping with AuNP, band gap of GO increased and indicates its degradation in visible light. Optimum pH value was found to be 5.5 and adsorbent dose was 2.0 g/L. Adsorption kinetic data were best fitted with pseudo-second-order kinetic model, suggesting hydrogen bonding as well as ionic interactions of 2, 4-D on GO/AuNP-g-VTMS-Co-IA/HEMA. The efficiency of the photocatalyst was tested for its regeneration and reusability for five cycles. The method of synthesis may be extended to design more graphene-based composites for various applications in the field of catalysts, bio-molecule sensor, and nano-electronic devices. These features make the GO/AuNP-g-VTMS-Co-IA/HEMA a recommendable candidate for applications related to environmental aqueous pollution.

References

[1] R.R. Solis, F.J. Rivas, A.M. Piernas, A. Aguera, Ozonation, photocatalysis and photocatalytic ozonation of diuron intermediate identification, Chemical Engineering Journal, 292 (2016) 72-81.

[2] K. James, W.D Guenzi (Eds). Pesticide in soil and water, American Soil Science Society, Madison, WI 1986.

[3] M. Kumar, R. Tamilarasan, S. Sivakumar, Adsorption of Victoria blue by carbon/Ba/alginate beads: kinetics, thermodynamics and isotherm studies, Carbohydrate polymer, 98 (2013) 505–513.

[4] P. Mondal, C.B. Majumder, B. Mohanty, J. Hazar, Laboratory based approaches for arsenic remediation from contaminated water: Recent developments, Journal of Hazardous Materials, 137 (2006) 464-479.

[5] V.C. Guota, T. Eren, N. Atar, M.L. Yola, C. parlak, H. K. Maleh, $CoFe_2O_4@TiO_2$ decorated reduced graphene oxide nanocomposites for photocatalytic degradation of chlorpyrifos, Journal of Molecular Liquids, 208 (2015)122-129

[6] T.S. Anirudhan, J.R. Deepa, Binusreejayan, Electrochemical sensing of cholesterol by molecularity imprinted polymer of silyated graphene oxide and chemically modified nanocellulose polymer, Material Science Engineering C, 92 (2018) 942–956.

[7] J.R. Deepa, T.S. Anirudhan, G. Soman, V. C. Sekhar, Electrochemical sensing of methylmalonic acid based on molecularly imprinted polymer modified with graphene oxide and gold nanoparticles, Microchemical Journal, 313 (2020) 105489.

[8] T.S. Anirudhan, J.R. Deepa, Binusreejayan, Synthesis and characterisation of multicarboxyl functionalised nanocellulose/Nano bentonite composite for the adsorption of uranium (VI) from aqueous solutions, Chemical Engineering Journal, 273 (2015) 390–400.

[9] B. A. Fil, M. T. Yilmaz, S. Bayar, M. T. Elkoca, Investigation of adsorption of the dyestuff astrazon red violet 3rn (basic violet 16) on montmorillonite clay, Brazilian Journal of Chemical Engineering, 31 (2014) 171-182.

[10] D.R. Dreyer, S. Park, C.W. Bielanski, R.S. Ruoff. The chemistry of graphene oxide, Chemical Society Reviews, 39 (2010) 228-240.

[11] J.W. Jiang, J.S. Wang, B. Li, Young's modulus of graphene; A molecular dynamics study, Physical Review B, 80 (2009)113405-113408.

[12] H. Jin, H. Guo, X. Gao, R. Gui, Selective and sensitive electrochemical sensing of gastrodin based on Nickel foam modified with reduced graphene oxide/ silver nanoparticle complex-encapsulated molecularly, Sensors and Actuators B: Chem. 277 (2018) 14–21.

[13] D Y Cai, M.A Song, A Simple route to enhance the interface between graphite oxide nanoplatelets and a semi crystalline polymer for stress transfer, Nanotechnology, 20 (2009) 315708.

[14] S.A. Zaidi, Molecular imprinting polymers and their composites : a promising material for diverse applications, Biomaterials Science, 3 (2017) 388–402.

[15] S. Kalia, A. Dufresense, B.M. Cherian, B.S. Kaith, L. Averous, J. Njuguna, E. Nassiopoulos, Cellulose-Based Bio-and Nanocomposites: A Review, International Journal of Polymer Science, (2011) 117-131.

[16] S. Liwen, M. Liao, M. Sumiya, A comprehensive review of semiconductor ultraviolet photodetectors: from thin film to one-dimensional nano structures, Sensors, 13 (2013) 10482-10518.

[17] X. H. Ji, X. N. Song, J. Li, Y. B. Bai, W. S. Yang and X. G. Peng, Size control of gold nanocrystals in citrate reduction: the third role of citrate, Journal of American Chemical Society, 129 (2007) 13939–13948.

[18] T.S. Anirudhan, J.R. Deepa, S. Nisha, Fabrication of molecularly imprinted silyted graphene oxide polymer for sensing and quantification of creatinine in blood and urine samples, Applied Surface Science, 466 (2019) 28–39.

[19] H. Jin, H. Guo, X. Gao, R. Gui, Selective and sensitive electrochemical sensing of gastrodin based on nickel foam modified with reduced graphene oxide/silver nanoparticles complex-encapsulated molecularly, Sensors and Actuators B: Chem. 277 (2018) 14–21.

[20] H. Dong, W. Gao, F. Yan, H. Ji, H, Fluorescence resonance energy transfer between quantum dots and graphene oxide for sensing biomolecules, Analytical Chemistry, 82 (2010) 5511–5517.

[21] T.S. Anirudhan, J.R. Deepa, Anoop S. Nair, Fabrication of chemically modified graphene oxide /nano hydroxyapatite composite for adsorption and subsequent photocatalytic degradation of aureomycin hydrochloride, Journal of Industrial and Engineering Chemistry, 47 (2017) 415-430.

[22] T.S. Anirudhan, J.R. Deepa, Nano zinc oxide incorporated graphene oxide /nanocellulose composite for the adsorption and photo catalytic degradation of ciprofloxacin hydrochloride from aqueous solutions, Journal of Colloid and Interface Science, 490 (2017) 343–435.

[23] B. Li, T. Liu, Y. Wang, Z. Wang, ZnO/graphene oxide nanocomposite with remarkably enhanced visible- light -driven photocatalytic performance, Journal of Colloid and Interface Science, 377 (2012) 114–121.